

PERSPECTIVE

## Designing polymer coatings for lithium metal protection

To cite this article: Hongyao Zhou and Ping Liu 2022 *Nanotechnology* **33** 112501

View the [article online](#) for updates and enhancements.

### You may also like

- [Preparation and characterization of PTFE coating in new polymer quartz piezoelectric crystal sensor for testing liquor products](#)  
Yu Gu, , Qiang Li et al.
- [Enhancing infrared emission behavior of polymer coatings for radiative cooling applications](#)  
Meijie Chen, Dan Pang, Xingyu Chen et al.
- [The Electrical Properties of Protective Polymer Coatings as Related to Corrosion of the Substrate](#)  
Martin W. Kendig and Henry Leidheiser



The Electrochemical Society  
Advancing solid state & electrochemical science & technology

242nd ECS Meeting

Oct 9 – 13, 2022 • Atlanta, GA, US

Abstract submission deadline: **April 8, 2022**

Connect. Engage. Champion. Empower. Accelerate.

**MOVE SCIENCE FORWARD**



Submit your abstract



## Perspective

# Designing polymer coatings for lithium metal protection

Hongyao Zhou<sup>1,\*</sup> and Ping Liu<sup>2,\*</sup>

<sup>1</sup> Department of Chemistry, The University of Tokyo, 7-3-1 Hongo, Bunkyo-ku, Tokyo 113-0033, Japan

<sup>2</sup> Department of Nanoengineering, University of California San Diego, La Jolla, CA 92093, United States of America

E-mail: [hozhou@chem.s.u-tokyo.ac.jp](mailto:hozhou@chem.s.u-tokyo.ac.jp) and [piliu@eng.ucsd.edu](mailto:piliu@eng.ucsd.edu)

Published 23 December 2021

## Abstract

Protection of lithium metal has been one of the great challenges to realize a long-life, high-energy-density battery. Polymer coatings on lithium metal surface have been proven to be an effective protection method in terms of improved morphology, higher coulombic efficiency, and a longer cycle life. However, there is a variety of design principles of polymer coatings proposed by the research community, and the influence of polymer swelling in liquid electrolytes remains poorly understood. Herein we use crosslinking density and solvent–polymer interaction to quantitatively explain the mechanical property and the ion-transport property of polymer coatings when swollen in liquid electrolytes. Low crosslinking density is beneficial for reducing the rigidity and enhancing the viscosity of the polymer. Ion conductivity increases with the swelling ratio, and activation energy of lithium-ion transport increases in a polar polymer with strong ion–polymer coupling. We propose that polymer coatings must be combined with the emerging electrolytes with unconventional solvent compositions to realize a practical high-performance lithium metal battery. This study can provide design guidelines for polymer coatings through the optimized interactions with upcoming high-performance electrolytes.

Keywords: polymer coating, rechargeable lithium metal battery, energy storage

(Some figures may appear in colour only in the online journal)

## Abbreviations

SEI	solid electrolyte interface
CE	coulombic efficiency
SHP	self-healing polymer
MD	molecular dynamics
OCV	open-circuit voltage
LiTFSI	lithium bis(trifluoromethanesulfonyl)imide
LiFSI	lithium bis(fluorosulfonyl)imide
LiPF <sub>6</sub>	lithium hexafluorophosphate
LiF	lithium fluoride
Li <sub>2</sub> CO <sub>3</sub>	lithium carbonate
Li <sub>2</sub> S <sub>3</sub>	lithium trisulfide
LiNO <sub>3</sub>	lithium nitrate
PAN	polyacrylonitrile
PAN–PBD	poly(acrylonitrile-co-butadiene)
PIM	polymer of intrinsic microporosity
PEO	poly(ethylene oxide)
PVDF	poly(vinylidene fluoride)
PMMA	poly(methyl methacrylate)
PyTFSI-FA	poly(pyrrolidinium bis(trifluoromethanesulfonyl)imide-co-1H, 1H-heptafluorobutyl acrylate)

\* Authors to whom any correspondence should be addressed.

PEO-Upy	poly(ethylene oxide-co-ureidopyrimidinone)
CMP	conjugated microporous thermosetting polymer
SPEEK	sulfonated polyether ether ketone
FTEG	perfluoro-tri(ethylene glycol)
EC	ethylene carbonate
DMC	dimethyl carbonate
DEC	diethyl carbonate
FEC	fluoroethylene carbonate
FEMC	3,3,3-fluoroethylmethyl carbonate
HFE	1,1,2,2-tetrafluoroethyl-2',2', 2'-trifluoroethyl ether
DOL	1,3-dioxolane
DME	dimethoxyethane
DEE	diethyl ether
BTFE	bis(2,2,2-trifluoroethyl)ether
TTE	1,1,2,2-tetrafluoroethyl-2,2,3,3-tetrafluoropropyl ether
DMSO	dimethyl sulfoxide
SL	sulfolane

## 1. Introduction

Lithium (Li) metal battery offers the highest possible energy density in Li ion-based chemistries by using the direct plating/dissolution process of metallic Li on the anode side. The specific capacity of Li metal anode is no longer limited by the capacity of the host materials (e.g. graphite) for Li intercalation. The theoretical capacity of Li metal anode is  $3860 \text{ mAh g}^{-1}$ , a ten-times greater value compared to the graphite anode [1, 2].

The challenges for Li metal anode, however, are the instability with the electrolyte and the non-uniform (dendritic) growth of metallic Li. Recently, the stability of Li metal anode has been dramatically enhanced through electrolyte engineering, and multiple studies have reported very high coulombic efficiency (CE) of Li plating/stripping cycle reaching above 99%. The high stability of Li metal relies greatly on the robust solid electrolyte interface (SEI) layer formed between the Li metal and the electrolyte [3–9].

To make Li metal battery as a commercially valuable product, and to replace the existing intercalation-based graphite anode, the CE of Li plating/stripping cycle must achieve 99.7% (calculation based on the requirements to achieve  $500 \text{ Wh kg}^{-1}$  battery) [1, 10]. This goal demands extremely low reactivity between Li and the electrolyte. Relying only on the intrinsic SEI layer produced from the electrolyte decomposition might be insufficient to achieve the target CE value, because the large volume change of Li metal might break the SEI layer in every deposition/stripping cycle, and the exposed Li metal will continue to react with the electrolyte until Li is covered again with a newly formed SEI layer [11].

Protective coating (or artificial SEI layer) is an ion-conductive layer covered on a fresh Li metal electrode to enhance the stability of Li metal (figure 1). Spherical morphologies of Li deposits are often observed underneath the coating layer, which suggests the coating layer can alter the nucleation and growing process of Li metal [12].

In a 2020 review article of protective coatings, we proposed two major protection schemes: mechanical suppression of Li dendrites, and chemical selectivity for  $\text{Li}^+$  cation [10]. We categorized inorganic and polymeric coating materials

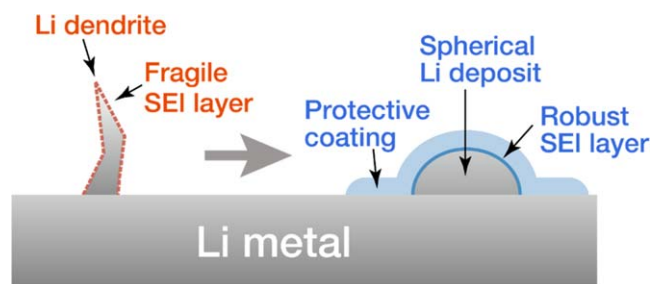


**Figure 1.** Scheme of a protective coating on Li metal anode, which improves the morphology of plated Li and the robustness of SEI layer.

based on their ion conductivity, Young's modulus, and polarity (i.e. Hildebrand solubility parameter). Li metal underneath a protective coating undergoes a significant volume change during the plating/stripping cycles. Therefore, a uniform surface coverage and high resilience to the repetitive volume change is very important to avoid the coating failure.

Polymeric materials have a clear advantage over inorganic materials, thanks to the flexible and elastic nature of polymers. The simple coating process of polymer materials is scalable and cost-effective. In the previous review article, we pointed out that the physical properties of polymeric coatings (unlike non-swelling inorganic coatings) can change after the immersion in the liquid electrolyte [10]. As a proof of concept, we experimentally demonstrated in a recent study that ion-transport properties are closely related to the swelling ratio and solvent–polymer interaction and provided the mathematical descriptions to quantify those parameters [13].

In this perspective article, we first introduce the fundamental descriptors of protective polymer coatings and then evaluate the validity of our theory by applying those descriptors to recent studies on polymer coatings. Finally, we expect that our theory can guide the future design of polymer coatings which are compatible with the state-of-the-art electrolyte. Such a polymer–electrolyte combination can deliver a synergistic improvement on Li metal anode.

## 2. Controlling parameters of polymer coatings

The physical properties and the protective function of polymer coatings can be described in terms of crosslinking density, solvent–polymer interaction, and chemical stability with lithium metal (figure 2). These three parameters then govern mechanical and ion-transport properties of the coatings.

### 2.1. Crosslinking density

The equilibrium swelling ratio of polymer coatings is limited by degree of chemical crosslinking between the polymer chains. The crosslinking density ( $N$ ) can be evaluated from Flory–Rehner equation [13, 14]:

$$N = \frac{\ln(1 - v_2) + v_2 + \chi v_2}{V_1(v_2/2 - v_2^{1/3})}. \quad (1)$$

Subscript 1, and 2 denotes that the parameter is related to the solvent, and the polymer, respectively.  $V_1$  is the molar volume of the solvent,  $v_2$  is the volume fraction of polymer in the swollen state, which equals the inverse of the swelling ratio ( $v_2 = V_0/V$ ;  $V_0$  and  $V$  are the volume of polymer before and after swelling, respectively), and  $\chi$  is solvent–polymer interaction parameter (see section 2.2).

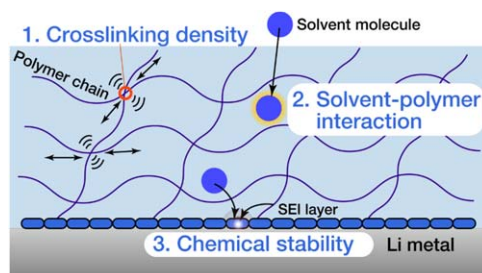


**Figure 2.** Three controlling parameters for the physical properties and the protective function of a polymer coating.

High crosslinking density generally results in low swelling ratio, and little electrolyte can permeate through the coating layer. Such a coating can block liquid electrolyte from reacting with the Li metal. However, the ionic conductivity drastically decreases under an extremely low solvent content, and the Li metal tends to grow from the local defects in the coating (where the local resistance is low), leading to failure of the protective function. More details are discussed in section 4.

This trade-off between crosslinking density and ion transport can be addressed by introducing the concept of dynamic crosslinking, which is formed by ionic bonding between the polymer chains. In contrast to conventional covalent crosslinking, the dynamic crosslinking can be reversibly attached or detached and provides the polymer coating a unique property such as liquid-like flowability or self-healing effect (see section 3).

### 2.2. Solvent–polymer interaction

The degree of interaction between solvent molecules and polymer chains can be quantified by the  $\chi$  parameter [13, 15]:

$$\chi = \frac{\alpha V_1}{4RT} [4(\delta_{D1} - \delta_{D2})^2 + (\delta_{P1} - \delta_{P2})^2 + (\delta_{H1} - \delta_{H2})^2] \quad (2)$$

$\alpha$  is an empirical parameter ( $\alpha = 0.6$  is often used),  $R$  is the standard gas constant, and  $T$  is temperature. The three  $\delta$  values represent Hansen solubility parameters (HSPs), which account for dispersion force ( $\delta_D$ ), dipole–dipole interaction ( $\delta_P$ ), and hydrogen-bonding ( $\delta_H$ ), respectively.

When the HSPs of polymer is close to the values of solvents, the polymer likely dissolves in the solvent. Therefore, the swelling ratio increases with reducing values of the  $\chi$  parameter. This relation can be intuitively understood by the ‘like dissolves like’ rule, commonly used in solution chemistry.

The HSPs of common polymers and solvents are readily available [15], and the HSPs of mixed solvents or copolymers are simply the linear combinations of the corresponding HSPs of pure solvents or homopolymers. HSPs offers a convenient way to estimate the value of  $\chi$  and the swelling ratio of polymer coatings.

### 2.3. Chemical stability

Thickness of the SEI layer on Li metal is generally a few tens of nanometers, and the major inorganic compounds found in the TEM observations include LiF [3–9],  $\text{Li}_2\text{CO}_3$  [16], and lithium methyl carbonate [17, 18]. LiF is believed to be the most effective compound in the SEI layer and produced from fluorinated salt such as LiTFSI, LiFSI, and  $\text{LiPF}_6$ , or fluorinated solvents such as FEC. Recently, a polymer coating bearing sulfonyl fluoride group ( $-\text{SO}_2\text{F}$ ) was reported to produce a dense LiF layer on Li metal surface [19].

The swelling ratio of a polymer coating decides the ratio among polymer, solvent, and salt at the Li metal surface. Therefore, when both electrolyte and polymer can be reduced by Li metal, the swelling ratio significantly influences the chemical composition of the SEI layer. For example, XPS analysis revealed that a PAN coating with higher crosslinking density (lower swelling ratio) results in a higher nitrogen content (from the decomposition of PAN) in the SEI layer [13].

#### 2.4. Coating techniques

Coating techniques have a major influence on the film thickness, uniformity, and scalability (coating area). A wide variety of coating techniques have been used for Li metal protection (detailed descriptions of these coating techniques are summarized in our previous review [10]). Briefly, the coating techniques can be categorized by two criteria: (1) gas phase versus solution phase precursors; (2) reactive versus inert precursors.

Molecular layer deposition (MLD) uses gas phase precursors and forms a nanometer-thick coating directly on Li metal [20]. The coating thickness can be precisely controlled by the number of MLD cycles. For example, a 4 nm-thick polyurea film was directly coated on Li metal surface by the MLD method [21]. Disadvantages of MLD method are the high processing cost and the poor scalability because the coating area is limited by the chamber size of the MLD system.

Spin coating produces a uniform polymer film from solution phase precursors [22, 23]. By adjusting the rotation speed, viscosity and surface tension of the solution, a wide range of thickness (typically 100 nm ~ 10  $\mu$ m) can be produced. Dip coating and blade casting are more scalable and more convenient techniques than spin coating if the desired film thickness is at the micrometer scale [24, 25].

Reactive precursors can react with Li metal to form a protective interlayer at the polymer–Li interface. The most popular interlayer produced by this technique is LiF (e.g. from PVDF [26], poly(SL-DOL) [19]). Because the surface reaction is self-terminated, a uniform interlayer can be obtained with a few tens of nanometer thickness [19]. In contrast, inert precursors undergo no side reaction with Li metal, and therefore, is suitable for the experiment when the chemical reaction with Li metal is unwanted. For example, inert polymer such as PDMS was used as the coating layer [23, 27] or as the substrate layer [28] to evaluate the mechanistic influence of the polymer layer on the Li metal morphology.

### 3. Mechanical property

#### 3.1. Viscoelasticity and resilience of polymer coating

The resilience of a polymer coating can be evaluated by elasticity and viscosity, which can be measured by rheological techniques. The elastic property is expressed by storage modulus ( $G'$ ) and is often modelled with a 'spring'.  $G'$  corresponds to the spring constant in Hook's law, and a large  $G'$  value means the coating exerts a large stress toward the opposite direction of growing Li metal. The viscous property is expressed by loss modulus ( $G''$ ) and is modelled with a 'dashpot'.  $G''$  corresponds to the dynamic viscosity, and a large  $G''$  value means the coating behaves like a liquid and deforms in response to the volume change of Li metal. This 'flowability' or 'adaptive nature' of the coating is beneficial for the uniform surface coverage and for filling in the void between the Li metal and the coating which is produced during the Li stripping step.

Bao group has been studying on the polymer designs maximizing the flowability ( $G''$  value) of the coatings [29, 30]. For example, ionic crosslinking between an  $Al^{3+}$  cation as the coordination centre and four anionic FTEG chains produces a flowable polymer coating, Al-FTEG (figure 3(a)) [29]. The crosslinks between

$\text{Al}^{3+}$  and FTEG is reversible (dynamic crosslinking) and Al-FTEG shows fluidic property at sufficiently slow shear rate, as evidenced by rheological analysis showing  $G' > G''$  below 20 Hz (figure 3(b)). The Al-FTEG film exhibits self-healing ability, and a scratch on the film completely disappeared after 12 h (figure 3(c)).

The mechanical property of polymer coatings can be classified into two categories, based on the relation between  $G'$  and  $G''$ :

- (1)  $G' < G''$  — the polymer film is flowable and shows self-healing ability. To repair any crack created during the Li plating, the self-healing rate must be faster than the growing rate of Li metal deposits.
- (2)  $G' \gg G''$  — the polymer film is classified as a gel and behaves like a solid [31]. Lower  $G'$  value results in softer and more resilient coating, while higher  $G'$  value results in harder and more rigid coating. Generally, the  $G'$  value increases with decreasing solvent content in the polymer coating, which is ultimately governed by the crosslinking density (see section 3.2).

### 3.2. Influence of crosslinking density on the rheology

Rheological property of polymer coatings can be influenced by the crosslinking density, because the interchain crosslinks restrict the polymer deformation. An amine-based self-healing polymer (SHP) was prepared by mixing the carbonyl-acid-terminated oligomer, diethylene triamine, and urea (figure 3(d)) [32]. Hydrogen bonding between the urea groups results in dynamic crosslinking, and the polymer exhibits self-healing property. The crosslinking density of the SHP was controlled by varying the concentration of triacid (1-X in figure 3(d)), and the rheological property was investigated (figure 3(e)). At a low triacid concentration (16%), the  $G'$  value was much lower than the  $G''$  value, which indicates the polymer is very flowable. The difference between the  $G'$  and  $G''$  decreases with increasing triacid concentration. At 70% of triacid, the  $G'$  and  $G''$  converge to almost the same value, and the polymer turns into a more rigid and solid-like material. This result demonstrates that crosslinking density of polymer coatings is a deciding parameter for the mechanical property. To note, rheology of the above Al-FTEG and amine-based SHP materials was evaluated in their dry states, and the values under the swollen state in liquid electrolyte was not measured.

In another study, we prepared covalently crosslinked PAN–PBD film, and the crosslinking density was controlled by the concentration of the crosslinking initiator ( $\text{Li}_2\text{S}_3$ ) (figure 4(a)). As a result, we confirmed that an increase of crosslinking density increases the  $G'$  and decreases the  $G''$  values (the polymer becomes more rigid), when the polymer was swollen in both ether and carbonate electrolytes [13].

We studied how the rheological property affected the morphology of Li metal. Li metal was electrochemically plated on a Cu substrate under the PAN–PBD coating layer with various crosslinking density. Interestingly, the plated Li metal was observed underneath the coating layer when the crosslinking density was low ( $\text{Li}_2\text{S}_3/\text{AN} \leq 0.3$ ), and on top of the coating layer when the crosslinking density was high ( $\text{Li}_2\text{S}_3/\text{AN} \geq 0.4$ ) (figure 4(b)). The Li metal underneath the poorly crosslinked PAN–PBD coating layer exhibited spherical morphology, in contrast to the dendritic shape observed on the uncoated Cu substrate (figure 4(c)). This result shows the clear benefit of a soft polymer coating to mitigate Li dendrite formation.

The penetration of Li metal through the PAN–PBD layer with a high crosslinking density may reflect the rigid and brittle nature of the coating, which is prone to the crack formation and less adaptive to the volume change of Li metal underneath. In addition to the poor mechanical property, we have found that the

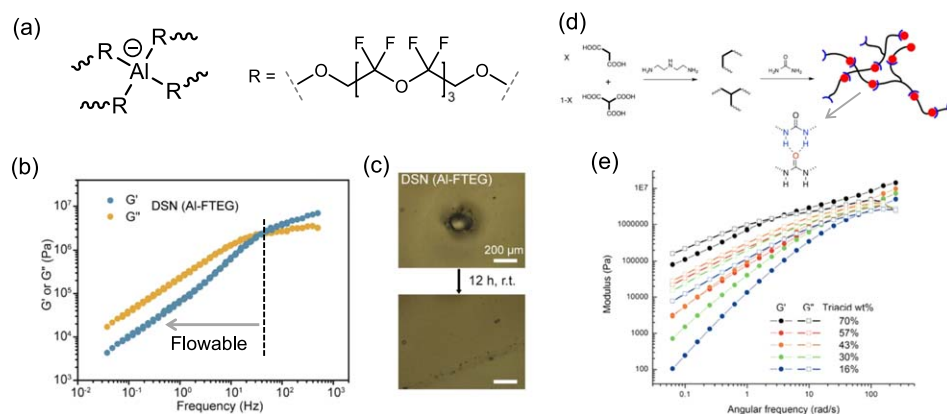


**Figure 3.** (a) Molecular structure of Al-FTEG (b) Rheology of Al-FTEG showing flowable property (c) Self-healing property of Al-FTEG. Reprinted from [29], © 2019 Published by Elsevier Inc. (d) Amine-based SHP dynamically crosslinked by hydrogen bonding between urea groups (e) Increasing modulus of SHP with increasing concentration of triacid (crosslinker, 1-X). Reprinted with permission from [32]. Copyright © 2016, American Chemical Society.

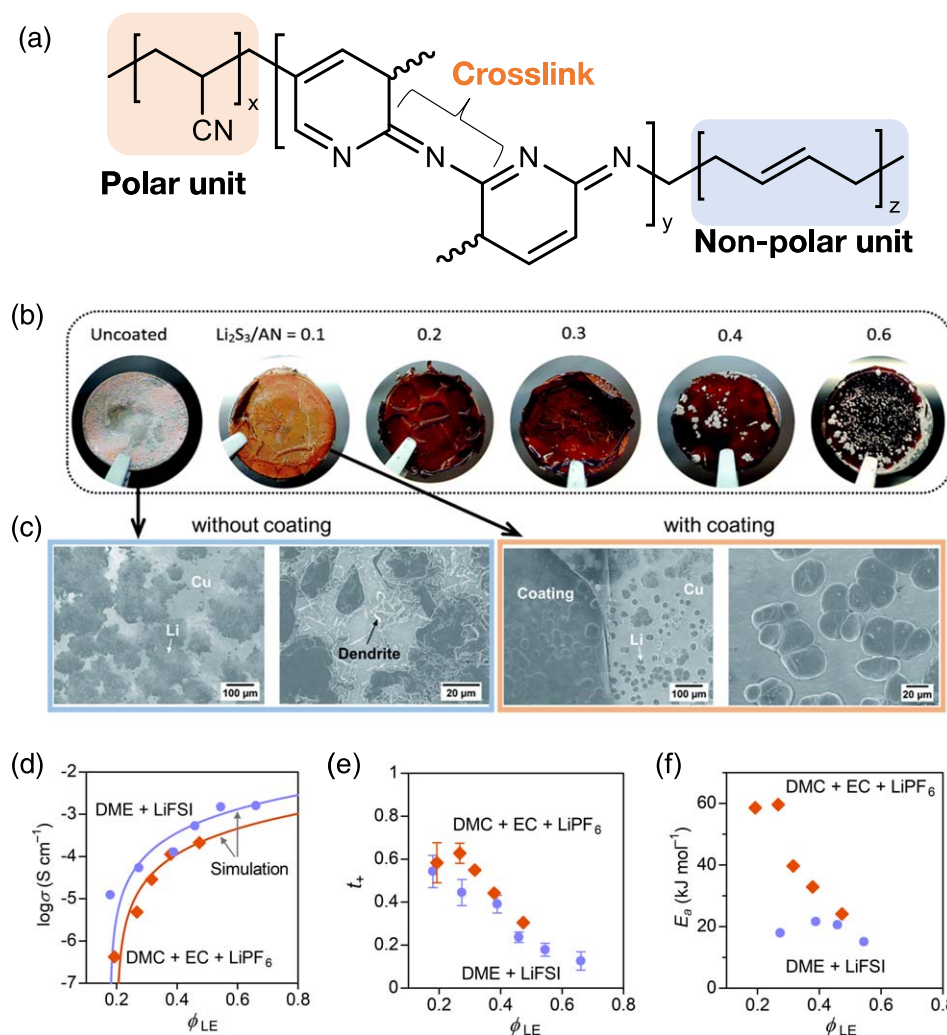


**Figure 4.** (a) Molecular structure of crosslinked PAN-PBD (b) Li metal electroplated with PAN-PBD coating crosslinked under varied  $\text{Li}_2\text{S}_3/\text{AN}$  ratio (increasing  $\text{Li}_2\text{S}_3/\text{AN}$  ratio results in higher crosslinking density, current =  $0.1 \text{ mA cm}^{-2}$ , capacity =  $1 \text{ mAh cm}^{-2}$ ) (c) SEM images of the electroplated Li metal with or without PAN-PBD coating ( $\text{Li}_2\text{S}_3/\text{AN} = 0.1$ ) (d) Ion conductivity, (e)  $\text{Li}^+$  transference number, and (f) activation energy of PAN-PBD coating under varied volume fractions of the liquid electrolyte ( $\phi_{\text{LE}}$ ). Reproduced from [13] with permission from the Royal Society of Chemistry.

significant reduction in ion conductivity simultaneously leads to the failure of coating layer (see section 4).

#### 4. Ion-transport property

Ion transport through the swollen polymer coating is generally mediated by the solvent molecules (except for the case in which  $\text{Li}^+$  is solely solvated by the polymer chains). Therefore, ion transport properties such as ion conductivity ( $\sigma$ ),  $\text{Li}^+$  transference number ( $t_+$ ), and activation energy ( $E_a$ ) must be governed by volume fraction of the liquid electrolyte absorbed inside the polymer coating ( $\phi_{\text{LE}}$ ). Further, the solvent–polymer interaction ( $\chi$  parameter) decides the  $\phi_{\text{LE}}$  in liquid electrolytes having different polarities.

Crosslinked PAN–PBD is an ideal platform to quantify the ion-transport properties as functions of crosslinking density and polarity of the liquid electrolyte (figures 4(d)–(f)) [13]. Evaluation of the  $\chi$  parameter using equation (2) in the two most common electrolytes indicates the preferential solvation of PAN phase in the carbonate electrolyte (high polarity), and PBD phase in the ether electrolyte (low polarity), respectively. The result reflects the large difference in polarity between PAN (polar) and PBD (non-polar) phases. Therefore, the solvation environment for  $\text{Li}^+$  cation is completely different between the carbonate and ether electrolytes.

Helms and co-workers focused more on the diversity of  $\text{Li}^+$ -coordinating side groups which is attached on spiro-bis(catechol) type polymers with intrinsic microporosity (PIMs, figure 5(a)) and studied the ion-transport properties [33]. Here we summarize the results obtained from these two studies using PAN–PBD and PIMs, respectively.

##### 4.1. Ion conductivity

The value of  $\sigma$  in PAN–PBD coating swollen in carbonate (EC:DMC (1:1) + 1 M  $\text{LiPF}_6$ ) and ether (DME + 1 M  $\text{LiFSI}$ ) electrolytes both follows the percolation model [13]:

$$\sigma = \sigma_0(\phi_{\text{LE}} - \phi_0)^n \quad (3)$$

$\sigma_0$  is a constant value,  $\phi_0$  is a percolation limit, and  $n$  is a universal constant ranging between 1.3 and 2 for a three-dimensional system ( $n = 2$  was used for the simulation curves in figure 4(d)). Equation (3) shows the  $\sigma$  value drastically decreases to zero when  $\phi_{\text{LE}}$  approaches  $\phi_0$ . Therefore, a polymer coating must absorb sufficiently large amount of liquid electrolyte (i.e.  $\phi_{\text{LE}} \gg \phi_0$ ) to maintain high ion conductivity. Otherwise, a poorly swollen polymer coating hinders uniform ion flux through the entire coating surface and exacerbates the non-uniform Li plating at local hot spots, breaking the coating layer (figure (b),  $\text{Li}_2\text{S}_3/\text{AN} \geq 0.4$ ).

The  $\sigma$  value of PIMs was evaluated in a carbonate electrolyte (EC:DEC (1:1) + 10% FEC + 1% VC + 1 M  $\text{LiPF}_6$ ). Interestingly, PIM-13 and -14 bearing both ternary amine and ether groups show the highest conductivity (figure 5(b)). The authors of the original study attributed the high conductivity to the coordination of amine and ether groups on  $\text{Li}^+$  cation and the unique local dielectric environment created around it. In addition, we posit that the functional groups on PIMs have a great influence on the swelling ratios of the polymer film.

Ion conductivity is also influenced by the coating thickness. Excessively thick polymer coatings can block the  $\text{Li}^+$  ion transport and should be avoided. For example, poor conductivity of a thick Nafion coating (9  $\mu\text{m}$  thick) resulted in dendritic Li deposition from the local hotspot and broke the coating [34]. A thinner Nafion coating (200 nm), on the other hand, allows  $\text{Li}^+$  ion transport

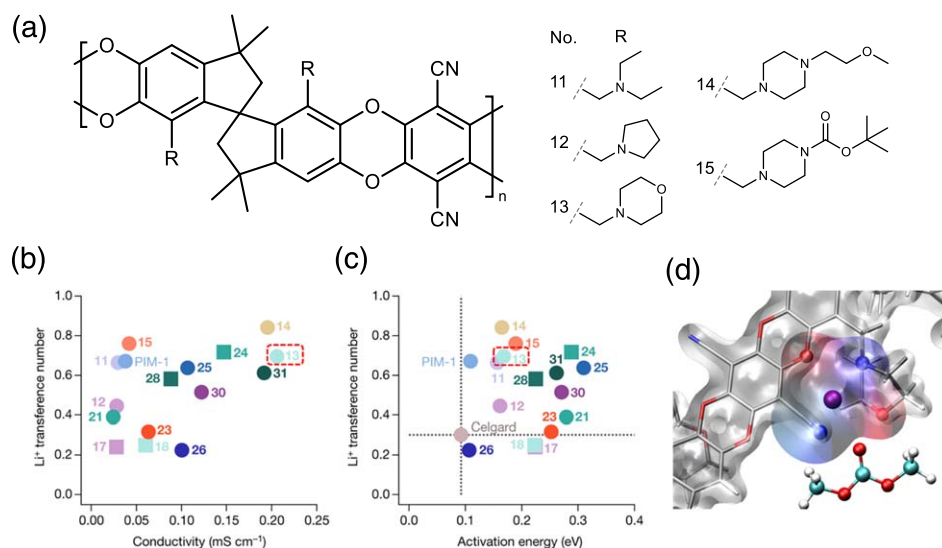


**Figure 5.** (a) Molecular structure of PIMs with various side groups (R of only No. 11 ~ 15 is shown) (b) Li<sup>+</sup> transference number versus ion conductivity, and (c) Li<sup>+</sup> transference number versus activation energy of PIMs family (d) 3D structure of PIM-13 and the solvation structure around Li<sup>+</sup> cation (purple sphere). Reproduced from [33] with permission from the Nature Publishing Group.

through the coating layer, and Li deposited underneath the coating. Finally, a conductive coating (with high swelling ratio) can be used even at a very large thickness, while a resistive coating (with low swelling ratio) should be used at a minimum thickness.

#### 4.2. Transference number

The value of  $t_+$  in PAN–PBD coating increased with decreasing value of  $\phi_{LE}$  for both carbonate and ether electrolytes (figure 4(e)). At high  $\phi_{LE}$ , the  $t_+$  value is low because the strong coordination of the solvent molecules around Li<sup>+</sup> cation increases the solvation radius and reduces the cation mobility. With the reduction of  $\phi_{LE}$ , the solvation radius decreases, and the relative mobility of intrinsically small Li<sup>+</sup> cation ( $= t_+$ ) increases.

Among PIMs family, PIM-14 and -15 bearing the piperazine ring showed the highest value of  $t_+ = 0.8$  (figure 5(c)). A comparison with the low  $t_+$  value ( $=0.3$ ) for Celgard (a microporous polypropylene separator which does not coordinate with Li<sup>+</sup> cation) confirms that the polymer–ion interaction has the dominant influence on the  $t_+$  values of polymer coatings.

#### 4.3. Activation energy

The value of  $E_a$  in PAN–PBD shows a strong dependence on polarity of the liquid electrolyte. In the polar carbonate electrolyte, the  $E_a$  value increases with  $\phi_{LE}$  when  $\phi_{LE}$  value is low, because of strong ion–dipole interaction between Li<sup>+</sup> cation and the nitrile group of PAN. On the other hand, little increase was observed in the less-polar ether electrolyte, because the non-polar PBD does not interact with Li<sup>+</sup> cation.

The  $E_a$  values of all PIMs family increased from the baseline evaluated with only Celgard (figure 5(c)). The high  $E_a$  indicates the polymer–ion interaction creates additional energy barrier in ion-transport. MD simulation was carried out to calculate the trajectory of and the energy barrier for the transporting Li<sup>+</sup> cation (figure 5(d)). The result shows Li<sup>+</sup> is partially coordinated with PIM-13, and a DMC solvent molecule coordinates to the other side of Li<sup>+</sup>. The predicted transport pathway shows that Li<sup>+</sup> cation hops between the two solvation cages created around the nitrile group and the morpholine ring. The highest energy

barrier ( $E_a = 0.24\text{--}0.27$  eV) lies in the dissociation step of  $\text{Li}^+$  from nitrogen and oxygen atoms.

In summary,  $E_a$  of polymer coatings strongly depends on both  $\phi_{\text{LE}}$  and polarity of the polymer. Non-polar polymers swollen in ether electrolytes can maintain low  $E_a$  values, thanks to the weak ion–polymer interaction. In contrast, polar polymers swollen in carbonate electrolytes have high  $E_a$  values, especially at low  $\phi_{\text{LE}}$ , because of the strong coupling between polymer and  $\text{Li}^+$  cation.

## 5. Perspectives for polymer coating study

### 5.1. *In-situ* observation of Li metal under the coating

Characterization of the SEI layer and morphological study of Li metal under a polymer coating have been carried out mainly in *ex-situ* experiments. However, given the instability of Li metal surface, the sample handling/preparation after the electroplating step could damage or alter the Li morphology and the composition of SEI layer. *In-situ* characterization, on the other hand, can avoid the unwanted damages to the sample. For example, *in-situ* TEM observation of Li growth was carried out in a sealed electrochemical cell with a liquid electrolyte inside, and the morphology of Li metal with/without cationic polymer coating was compared [35].

Another important characterization technique is *in-situ*  $^7\text{Li}$  NMR [36]. The intensity in  $^7\text{Li}$  NMR spectra corresponds to the abundance of Li metal in the cell (figure 6(a)). The remaining Li metal intensity at the end of the stripping step is attributed to ‘dead Li’, which is disconnected from the Cu current collector and electrochemically inaccessible [37]. Polymer coating of the Cu surface with PVDF and PMMA resulted in lower intensity of dead Li (figure 6(b)), while PEO coating showed no change in the dead Li intensity compared to bare Cu. The CE increased with PMMA coating compared to bare Cu, indicating PMMA successfully protected the Li metal surface (figure 6(c)). On the contrary, the CE decreased with a PVDF coating, suggesting that more Li metal was consumed in the SEI formation reaction.

Li metal is known to be consumed by galvanic corrosion even when the battery is at rest [38]. To quantify the amount of Li metal consumed during the OCV period, Li metal intensity was monitored at the end of Li plating step. The Li metal intensity decreased at a faster rate on bare Cu than on any other polymer-coated Cu (figure 6(d)). This result shows that any viscoelastic coating can delay the rate of galvanic corrosion. Specifically, PMMA coating showed the best protective function both in reducing the amount of dead Li and delaying the galvanic corrosion rate. In summary, *in-situ*  $^7\text{Li}$  NMR is very useful in evaluating the amount of dead Li and the rate of galvanic corrosion reduced by a polymer coating.

### 5.2. Combination with high-performance electrolyte

One of the important milestone for practical Li metal battery is to achieve CE above 99.7%. The values of CE reported in recent studies on Li metal protection by polymer coating are summarized in figure 7(a) and the detailed experimental parameters in table 1 [29, 30, 39–42].

The liquid electrolytes used in studies of polymer coatings are categorized into ether or carbonate-based electrolytes. The most common baseline electrolytes are: DOL + DME with LiTFSI and  $\text{LiNO}_3$  for ether-based electrolyte; and EC + DMC + FEC with  $\text{LiPF}_6$  for carbonate-based electrolyte. The highest CEs of 99.1% were observed in two reports, and both coatings were studied in the ether electrolyte. The higher CE values in the ether electrolyte than in the carbonate

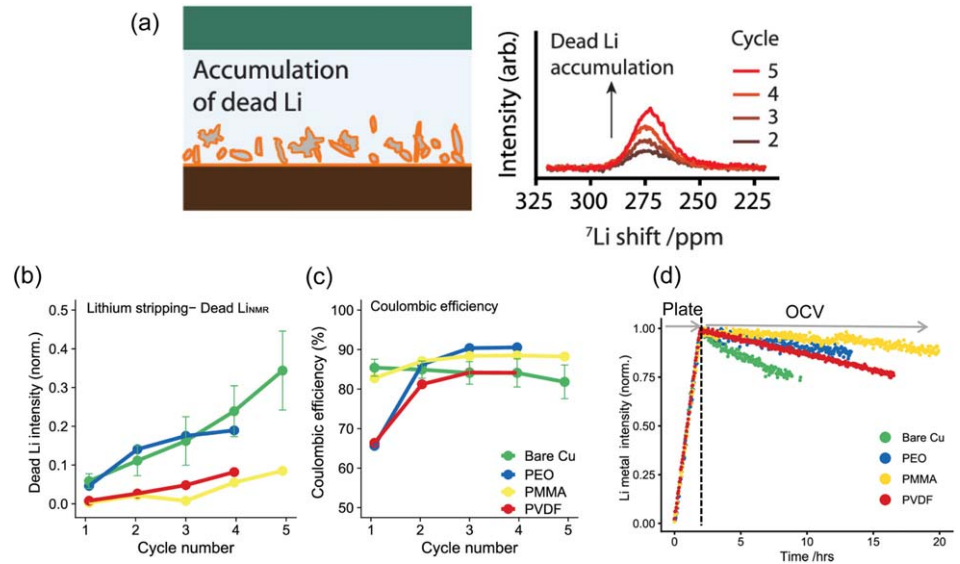


**Figure 6.** (a) Scheme of  $^7\text{Li}$  NMR analysis to quantify the amount of dead Li accumulated in the cell (b) NMR intensity of dead Li, and (c) CE of Li plating/stripping with various polymer coatings (c) Decrease of NMR intensity of Li metal at OCV. The intensity at the end of the plating step was normalized to one. Reproduced from [36]. CC BY 4.0.

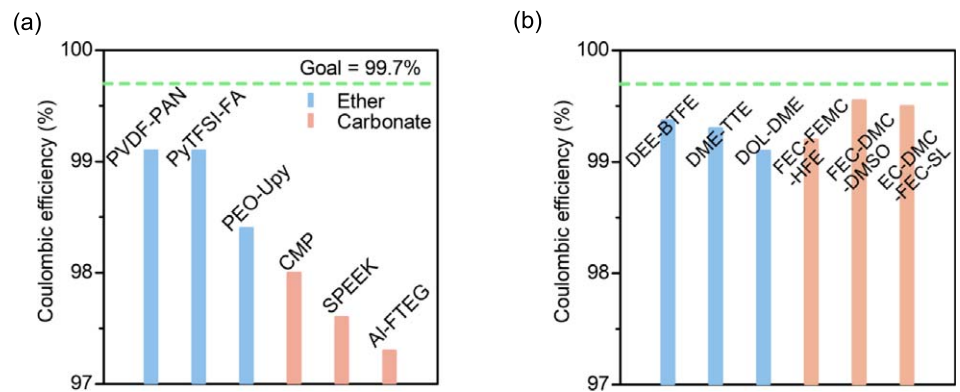


**Figure 7.** (a) CEs of Li plating/stripping in conventional liquid electrolytes with various polymer coatings (b) CEs of the state-of-the-art liquid electrolytes with unconventional solvent composition. The detailed compositions are shown in table 1.

electrolyte might just reflect the difference in stability of the baseline electrolytes (Li metal is more stable in ether than in carbonate). An intuitive idea is then to combine protective coatings with the state-of-the-art baseline electrolytes with higher CEs than what have been used before.

Recent advancement in electrolyte engineering for Li metal battery is remarkable. Figure 7(b) summarizes the CEs of new electrolytes reported in recent years [3–9]. The idea of localized high concentration electrolyte and fluorine-rich electrolyte have yielded very high CEs approaching 99.5%, both in ether and carbonate electrolytes. The requirement for the stability of polymer coating would be more stringent when used with those new electrolytes. Any side reaction between the polymer and Li metal would only deteriorate the CE. The new electrolytes often contains unconventional solvents such as perfluoroether or fluorocarbonate. Calculation of  $\chi$  parameter between the polymer and these solvents would be very helpful in estimating the swelling ratio and conductivity. We can also optimize the viscoelastic properties ( $G'$  and  $G''$  values) of the polymer coating by tailoring the crosslinking density and the swelling ratio. Further, MD simulation would be a powerful method to simulate the ion-transport pathway and

**Table 1.** Experimental parameters used in the evaluation of CEs shown in figures 7(a) and (b).

Coating	Electrolyte	Current (mA cm <sup>-2</sup> )	Capacity (mAh cm <sup>-2</sup> )	CE (%)	Cycle	References
Polymer coatings + Conventional electrolytes						
PVDF-PAN	DOL:DME (1:1) + LiTFSI (1 M) + LiNO <sub>3</sub> (5%)	1	1	99.1	450	[39]
PyTFSI-FA	DOL:DME (1:1) + LiTFSI (1 M) + LiNO <sub>3</sub> (1%)	0.5	1	99.1	10 <sup>a</sup>	[30]
PEO-Upy	DOL:DME (1:1) + LiTFSI (1 M) + LiNO <sub>3</sub> (2%)	1	1	98.4	150	[40]
CMP	EC:DMC (1:1) + LiPF <sub>6</sub> (1 M)	1	1	98	150	[41]
SPEEK	EC:DMC (3:2) + FEC (10%) + LiPF <sub>6</sub> (1 M)	1	3	97.6	140	[42]
Al-FTEG	EC:DEC (1:1) + FEC (10%) + LiPF <sub>6</sub> (1 M)	0.25	0.5	97.3	400	[29]
New electrolytes with unconventional solvent composition						
	DEE:BTFE (1:4) + LiFSI (1.8 M)	0.5	1	99.37	900	[3]
	DME:TTE:LiFSI (1.2:3:1)	0.5	1	99.3	300	[4]
	DOL:DME (1:1) + LiNO <sub>3</sub> (3%) + LiTFSI (1 M) + LiFSI (2 M)	0.5	1	99.1	450	[5]
	FEC:FEMC:HFE (1:3:1) + LiPF <sub>6</sub> (1 M)	0.2	1	99.2	500	[6]
	FEC:DMC (1:4) + 5% (4 M LiNO <sub>3</sub> in DMSO)	1	1	99.55	10 <sup>b</sup>	[8]
	EC:DMC (1:1) + LiPF <sub>6</sub> (1 M) + FEC (5%) + 5% (0.1 M LiNO <sub>3</sub> in SL)	0.5	0.5	99.5	10 <sup>b</sup>	[9]

*a, b:* Li metal was predeposited ( $a = 5 \text{ mAh cm}^{-2}$  or  $b = 3 \text{ mAh cm}^{-2}$ ) as a reservoir and completely stripped after 10 cycles.

to calculate the  $E_a$  in the swollen polymer coating. High throughput computational screening would allow us to identify the best polymer design for the new electrolytes. We believe that polymer coating is the last steppingstone to increase the CE of the liquid electrolyte to the target value.

### Acknowledgments

This work was supported by the Office of Vehicle Technologies of the US Department of Energy through the Advanced Battery Materials Research (BMR) Program (Battery500 Consortium) under Contract No. DE-EE0007764.

### Data availability statement

All data that support the findings of this study are included within the article (and any supplementary files).

### ORCID iDs

Hongyao Zhou  <https://orcid.org/0000-0002-5802-6276>

Ping Liu  <https://orcid.org/0000-0002-1488-1668>

### References

- [1] Liu J *et al* 2019 Pathways for practical high-energy long-cycling lithium metal batteries *Nat. Energy* **4** 180–6
- [2] Varzi A, Thanner K, Scipioni R, Di Lecce D, Hassoun J, Dörfler S, Altheus H, Kaskel S, Prehal C and Freunberger S A 2020 Current status and future perspectives of lithium metal batteries *J. Power Sources* **480** 228803
- [3] Liu H *et al* 2020 Ultrahigh coulombic efficiency electrolyte enables Li||SPAN batteries with superior cycling performance *Mater. Today* **42** 17–28
- [4] Ren X *et al* 2019 Enabling high-voltage lithium-metal batteries under practical conditions *Joule* **3** 1662–76
- [5] Qiu F, Li X, Deng H, Wang D, Mu X, He P and Zhou H 2019 A concentrated ternary-salts electrolyte for high reversible Li metal battery with slight excess Li *Adv. Energy Mater.* **9** 1803372
- [6] Fan X *et al* 2018 Non-flammable electrolyte enables li-metal batteries with aggressive cathode chemistries *Nat. Nanotechnol.* **13** 715–22
- [7] Xue W *et al* 2020 FSI-inspired solvent and ‘full fluorosulfonyl’ electrolyte for 4 v class lithium-metal batteries *Energy Environ. Sci.* **13** 212–20
- [8] Liu S *et al* 2021 An inorganic-rich solid electrolyte interphase for advanced lithium-metal batteries in carbonate electrolytes *Angew. Chem.—Int. Ed.* **60** 3661–71
- [9] Piao N *et al* 2021 Lithium metal batteries enabled by synergetic additives in commercial carbonate electrolytes *ACS Energy Lett.* **6** 1839–48
- [10] Zhou H, Yu S, Liu H and Liu P 2020 Protective coatings for lithium metal anodes: recent progress and future perspectives *J. Power Sources* **450** 227632
- [11] Ye H, Zhang Y, Yin Y-X, Cao F-F and Guo Y-G 2020 An outlook on low-volume-change lithium metal anodes for long-life batteries *ACS Cent. Sci.* **6** 661–71
- [12] Lopez J, Pei A, Oh J Y, Wang G-J J N, Cui Y and Bao Z 2018 Effects of polymer coatings on electrodeposited lithium metal *J. Am. Chem. Soc.* **140** 11735–44
- [13] Zhou H, Liu H, Xing X, Wang Z, Yu S, Veith G M and Liu P 2021 Quantification of the ion transport mechanism in protective polymer coatings on lithium metal anodes *Chem. Sci.* **12** 7023–32
- [14] Flory P J and Rehner J 1943 Statistical Mechanics of Cross-Linked Polymer Networks II. Swelling *J. Chem. Phys.* **11** 521–6
- [15] Hansen C M 2007 *Hansen Solubility Parameters* (Boca Raton, FL: CRC Press)
- [16] Zhou H, Liu H, Li Y, Yue X, Wang X, Gonzalez M, Meng Y S and Liu P 2019 *In situ* formed polymer gel electrolytes for lithium batteries with inherent thermal shutdown safety features *J. Mater. Chem. A* **7** 16984–91

- [17] Liu H, Zhou H, Lee B S, Xing X, Gonzalez M and Liu P 2017 Suppressing lithium dendrite growth with a single-component coating *ACS Appl. Mater. Interfaces* **9** 30635–42
- [18] Liu H, Wang X, Zhou H, Lim H-D, Xing X, Yan Q, Meng Y S and Liu P 2018 Structure and solution dynamics of lithium methyl carbonate as a protective layer for lithium metal *ACS Appl. Energy Mater.* **1** 1864–9
- [19] Gao Y *et al* 2019 Polymer–inorganic solid–electrolyte interphase for stable lithium metal batteries under lean electrolyte conditions *Nat. Mater.* **18** 384–9
- [20] Chen L, Huang Z, Shahbazian-Yassar R, Libera J A, Klavetter K C, Zavadil K R and Elam J W 2018 Directly formed alucone on lithium metal for high-performance Li batteries and Li-S batteries with high sulfur mass loading *ACS Appl. Mater. Interfaces* **10** 7043–51
- [21] Sun Y *et al* 2019 A novel organic ‘polyurea’ thin film for ultralong-life lithium-metal anodes via molecular-layer deposition *Adv. Mater.* **31** 1806541
- [22] Kang I S, Lee Y-S and Kim D-W 2014 Improved cycling stability of lithium electrodes in rechargeable lithium batteries *J. Electrochem. Soc.* **161** A53–7
- [23] Zhu B, Jin Y, Hu X, Zheng Q, Zhang S, Wang Q and Zhu J 2017 Poly(dimethylsiloxane) thin film as a stable interfacial layer for high-performance lithium-metal battery anodes *Adv. Mater.* **29** 1603755
- [24] Gao Y, Zhao Y, Li Y C, Huang Q, Mallouk T E and Wang D 2017 Interfacial chemistry regulation via a skin-grafting strategy enables high-performance lithium-metal batteries *J. Am. Chem. Soc.* **139** 15288–91
- [25] Luo J, Fang C C and Wu N L 2018 High polarity poly(vinylidene difluoride) thin coating for dendrite-free and high-performance lithium metal anodes *Adv. Energy Mater.* **8** 1701482
- [26] Lang J *et al* 2019 One-pot solution coating of high quality LiF layer to stabilize Li metal anode *Energy Storage Mater.* **16** 85–90
- [27] Liu K *et al* 2017 Lithium metal anodes with an adaptive ‘solid–liquid’ interfacial protective layer *J. Am. Chem. Soc.* **139** 4815–20
- [28] Wang X, Zeng W, Hong L, Xu W, Yang H, Wang F, Duan H, Tang M and Jiang H 2018 Stress-driven lithium dendrite growth mechanism and dendrite mitigation by electroplating on soft substrates *Nat. Energy* **3** 227–35
- [29] Yu Z *et al* 2019 A dynamic, electrolyte-blocking, and single-ion-conductive network for stable lithium-metal anodes *Joule* **3** 2761–76
- [30] Huang Z, Choudhury S, Gong H, Cui Y and Bao Z 2020 A cation-tethered flowable polymeric interface for enabling stable deposition of metallic lithium *J. Am. Chem. Soc.* **142** 21393–403
- [31] Almdal K, Dyre J, Hvidt S and Kramer O 1993 Towards a phenomenological definition of the term ‘gel’ *Polym. Gels Networks* **1** 5–17
- [32] Lopez J, Chen Z, Wang C, Andrews S C, Cui Y and Bao Z 2016 The effects of cross-linking in a supramolecular binder on cycle life in silicon microparticle anodes *ACS Appl. Mater. Interfaces* **8** 2318–24
- [33] Baran M J *et al* 2021 Diversity-oriented synthesis of polymer membranes with ion solvation cages *Nature* **592** 225–31
- [34] Tu Z, Choudhury S, Zachman M J, Wei S, Zhang K, Kourkoutis L F and Archer L A 2017 Designing artificial solid-electrolyte interphases for single-ion and high-efficiency transport in batteries *Joule* **1** 394–406
- [35] Lee S Y, Shangguan J, Shangguan J, Alvarado J, Betzler S, Harris S J, Doeff M M and Zheng H 2020 Unveiling the mechanisms of lithium dendrite suppression by cationic polymer film induced solid-electrolyte interphase modification *Energy Environ. Sci.* **13** 1832–42
- [36] Gunnarsdóttir A B, Amanchukwu C V, Menkin S and Grey C P 2020 Noninvasive *in situ* NMR study of ‘dead lithium’ formation and lithium corrosion in full-cell lithium metal batteries *J. Am. Chem. Soc.* **142** 20814–27
- [37] Fang C *et al* 2019 Quantifying inactive lithium in lithium metal batteries *Nature* **572** 511–5
- [38] Lin D, Liu Y, Li Y, Li Y, Pei A, Xie J, Huang W and Cui Y 2019 Fast galvanic lithium corrosion involving a Kirkendall-type mechanism *Nat. Chem.* **11** 382–9
- [39] Wang D, Liu H, Liu F, Ma G, Yang J, Gu X, Zhou M and Chen Z 2021 Phase-separation-induced porous lithiophilic polymer coating for high-efficiency lithium metal batteries *Nano Lett.* **21** 4757–64
- [40] Wang G, Chen C, Chen Y, Kang X, Yang C, Wang F, Liu Y and Xiong X 2020 Self-stabilized and strongly adhesive supramolecular polymer protective layer enables ultrahigh-rate and large-capacity lithium-metal anode *Angew. Chem.—Int. Ed.* **59** 2055–60
- [41] Zhang K *et al* 2021 A high-performance lithium metal battery with ion-selective nanofluidic transport in a conjugated microporous polymer protective layer *Adv. Mater.* **33** 1–9
- [42] Weng Y T *et al* 2019 An ultrathin ionomer interphase for high efficiency lithium anode in carbonate based electrolyte *Nat. Commun.* **10** 1–10